All whistlers are not created equally: Scattering of strahl electrons in the solar wind via particle-in-cell simulations

Shinji Saito[1] and S. Peter Gary[1]

Received 13 September 2006; revised 26 October 2006; accepted 21 November 2006; published 4 January 2007.

[1] Solar wind observations show that suprathermal electrons (70 eV $\lesssim$ Energy $\lesssim$ 1 keV) of the magnetic-field-aligned "strahl" component have broader pitch-angle distributions than are predicted by adiabatic theories of solar wind expansion. Magnetosonic-whistler fluctuations propagating toward the Sun at $\mathbf{k} \times \mathbf{B}_o = 0$ (where $\mathbf{B}_o$ is the background magnetic field) have a strong cyclotron resonance with suprathermal electrons propagating in the anti-Solar direction along $\mathbf{B}_o$. This resonance enables strong pitch-angle scattering; thus whistlers are a likely source of the observed strahl broadening. Particle-in-cell simulations in a magnetized, homogeneous, collisionless plasma of electrons and protons are used to study the response of a strahl-like electron component to whistler fluctuation spectra. If the whistler anisotropy instability is excited via the initial application of $T_\perp/T_\parallel > 1$ to the electron core component, the resulting electron scattering leads to strahl pitch-angle distributions which decrease in width as electron energy increases. In contrast, if a power spectrum of whistler fluctuations proportional to k^{-3} is initially applied to the simulations, the resulting electron scattering leads to strahl pitch-angle distributions which increase in width as electron energy increases. **Citation:** Saito, S., and S. P. Gary (2007), All whistlers are not created equally: Scattering of strahl electrons in the solar wind via particle-in-cell simulations, *Geophys. Res. Lett.*, *34*, L01102, doi:10.1029/2006GL028173.

1. Introduction

[2] In the solar wind near Earth, the relatively dense, relatively cool core electrons are strongly influenced by particle-particle collisions [*Phillips and Gosling*, 1990], so that the velocity distributions of this component are usually observed to be Maxwellian or bi-Maxwellian-like. Above about 70 eV, however, Coulomb collisions become so weak that suprathermal electron distributions can become distinctly non-Maxwellian.

[3] At energies from above 70 eV to about 1 keV, two electron components have been identified: the halo and the strahl. Both components are quite tenuous compared to the core [*Maksimovic et al.*, 2005], but they are very different in their velocity-space properties [*Gosling et al.*, 2001]. The halo is isotropic or nearly so [*Feldman et al.*, 1975], whereas the strahl is highly anisotropic [*Rosenbauer et al.*, 1977; *Feldman et al.*, 1978], appearing as a finger in velocity space pointing along the background magnetic field $\mathbf{B}_o$ away from the Sun. The strahl, which is thought to consist of hot coronal electrons and is the primary carrier of the solar wind heat flux, has been scattered so that its pitch-angle widths are broader than that of the very narrow beam which is predicted by the adiabatic theory of solar wind expansion. The halo is usually interpreted as electrons which have been strongly scattered; the quasi-isotropic character of the halo requires that the scattering has taken place not only between the Sun and the Earth, but also at distances well beyond 1 AU [*Gosling et al.*, 2001]. But the specific scattering mechanisms of both strahl and halo remain unidentified [*Maksimovic et al.*, 2005].

[4] Most observations up to several hundred eV show that the strahl becomes more anisotropic [e.g., *Feldman et al.*, 1978; *Lemons and Feldman*, 1983; *Pilipp et al.*, 1987] or retains the same anisotropy [*Hammond et al.*, 1996] as electron energy increases. But recent WIND spacecraft observations up to 1 keV of *Pagel et al.* [2005] and *Vocks et al.* [2005] show strahl pitch-angle distributions in the fast solar wind which become somewhat broader on average with increasing electron energy. Furthermore, *Pagel et al.* [2007], using observations from the ACE spacecraft showed that, for 29 events corresponding to strahl with relatively broad pitch-angle distributions and enhanced magnetic field fluctuations at frequencies $\lesssim$ 3 Hz, the pitch-angle width of the strahl increased on average as the electron energy increased.

[5] Suprathermal electrons have a cyclotron resonance with whistler fluctuations at $\mathbf{k} \times \mathbf{B}_o = 0$. In contrast, Alfvén-cyclotron fluctuations usually have damping which increases with wave number and do not attain the short wavelengths required for that resonance. Therefore, whistlers are the electromagnetic mode most likely to provide pitch-angle scattering of the suprathermals. *Vocks and Mann* [2003] and *Vocks et al.* [2005] used quasilinear theory to show that whistlers can strongly pitch-angle scatter solar wind suprathermals, and that such scattering leads to an electron velocity distribution which becomes more isotropic with increasing energy. However, these calculations assumed a fixed power spectrum of whistler fluctuations; it is important to show these results also are present in the more self-consistent calculations represented by particle-in-cell simulations.

[6] The source of enhanced whistlers determines the characteristics of their power spectrum, and it is the spectral properties that determine which electrons undergo wave-particle interactions, and how strongly they are scattered. There are at least three such sources: heat flux instabilities, core anisotropy instabilities, and wave-wave interactions. The first of these is not a likely contributor to electron scattering near 1 AU because, as argued by *Pagel et al.* [2007], dispersion theory based upon electron observations predicts no significant growth for whistler heat flux instabilities. On the other hand, processes such as compression

[1]Space Science and Applications Group, Los Alamos National Laboratory, Los Alamos, New Mexico, USA.

0094-8276/07/2006GL028173$05.00

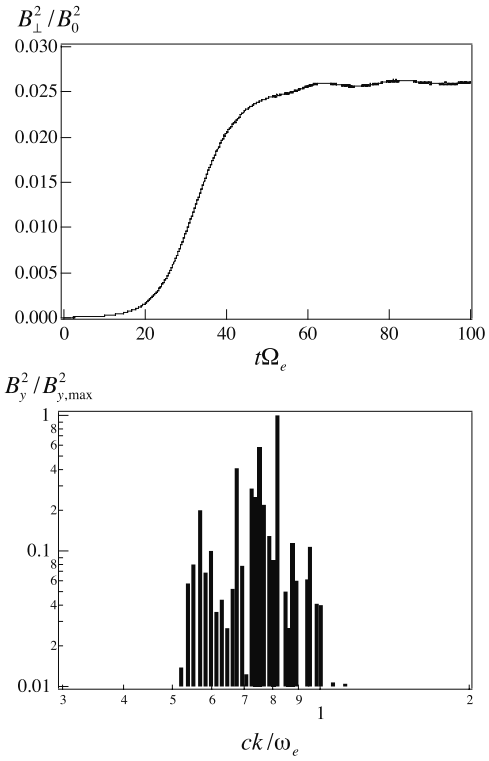

Figure 1. Simulation results for the whistler anisotropy instability run. (top) The normalized magnetic fluctuation field energy density as a function of time and (bottom) the power spectrum of the y-component of the fluctuating magnetic fields at $|\Omega_e|t = 50$ as a function of the parallel wave number.

due to interplanetary shocks may drive $T_\perp/T_\parallel > 1$ on the core (where the subscripts correspond to directions relative to $\mathbf{B}_o$) [*Phillips et al.*, 1989]; this anisotropy can, in turn, excite the whistler anisotropy instability which may be the source of the enhanced whistler fluctuations observed downstream of such shocks [*Pierre et al.*, 1995; *Lengyel-Frey et al.*, 1996]. Section 2 describes a particle-in-cell simulation in which such fluctuations scatter the suprathermals.

[7] Another potential source of enhanced whistlers are wave-wave interactions which lead, for example, to turbulent cascades and which, in turn, imply broadband power law magnetic fluctuation spectra in the whistler regime, as has been observed, for example, by *Beinroth and Neubauer* [1981] and *Smith et al.* [2006]. Section 3 describes a second simulation in which a broadband spectrum is applied at $t = 0$, and the subsequent electron responses are computed.

[8] We used a three-dimensional, fully relativistic, collisionless particle-in-cell electromagnetic simulation code [*Buneman*, 1993]. For both computations described below, the system is essentially one-dimensional, with spatial dimensions $L_x = 4096\Delta$, $L_y = 3\Delta$ and $L_z = 3\Delta$ where Δ is the grid size. For both simulations, the time step is $\delta t = 0.05/\omega_e$, the grid spacing is $\Delta = 0.10\ c/\omega_e$, $|\Omega_e|/\omega_e = 0.1$, and the plasma is homogeneous with periodic boundary conditions. Here the plasma frequency of the jth species is $\omega_j \equiv \sqrt{4\pi n_j e_j^2/m_j}$, and the cyclotron frequency of the jth species is $\Omega_j \equiv e_j B_o/m_j c$. Both simulations begin with three bi-Maxwellian electron components representing the core (subscript c), the strahl (s), and halo (h). The number of superparticles per cell is 85 for the core, 100 for the strahl, and 100 for the halo.

[9] The subscript e represents overall electron properties, i.e., $n_e = n_c + n_s + n_h$, $v_c = \sqrt{k_B T_{\parallel c}/m_e}$, and v_{oj} represents the magnetic-field-aligned average flow velocity of the jth component relative to the protons. We choose the following initial parameters: $m_p/m_e = 1836$, $\tilde{\beta}_{\parallel c} = 8\pi n_e k_B T_{\parallel c}/B_o^2 = 0.50$, $n_c/n_e = 0.85$, $n_s/n_e = 0.05$, $n_h/n_e = 0.10$, $v_{os}/v_c = -2.0$, $v_{oh}/v_c = +0.0$, $v_{oc} = -(n_s v_{os} + n_h v_{oh})/n_c$, $T_{\parallel c}/T_{\parallel p} = 1.0$, $T_{\parallel s}/T_{\parallel c} = 3.0$, $T_{\parallel h}/T_{\parallel c} = 10$, $T_{\perp c}/T_{\parallel c} = 3.0$ or 1.0, $T_{\perp s}/T_{\parallel s} = 0.10$, and $T_{\perp h}/T_{\parallel h} = 1.0$. Almost all of these parameters are consistent with typical observations in the solar wind near 1 AU. Untypical parameters include the relatively large strahl density, chosen to improve the suprathermal statistics, as well as the relatively large core anisotropy chosen in section 2 and the relatively large initial fluctuation level used in section 3, chosen to reduce computation time and to enhance the consequences of the scattering.

2. Simulation: Initially Anisotropic Electron Core

[10] This section describes a simulation of the whistler anisotropy instability, an electromagnetic mode driven unstable by the condition $T_{\perp e}/T_{\parallel e} > 1$. For a single, bi-Maxwellian electron velocity distribution, unstable modes typically arise at $\omega_p/c \ll k < \omega_e/c$ and $\Omega_p \ll \omega_r < |\Omega_e|$ [e.g., *Gary*, 1993, Figure 7.7], with maximum growth rate at $\mathbf{k} \times \mathbf{B}_o = 0$. The electrons most strongly resonant with this instability are those with $v_\parallel$ greater than the electron thermal velocity; a major consequence of this resonant interaction is pitch-angle scattering which reduces the overall anisotropy of the electron distribution [*Gary and Wang*, 1996].

[11] The simulation described in this section begins with the three component electron distribution described above, with $T_{\perp c}/T_{\parallel c} = 3.0$. Linear theory predicts that under these conditions the whistler anisotropy instability grows at propagation both parallel and anti-parallel to $\mathbf{B}_o$ with maximum growth rates $\gamma_m/|\Omega_e| \simeq 0.12$ (parallel) and 0.14 (antiparallel), at wave number $k_\parallel c/\omega_e \simeq 0.8$ with phase speed $\omega_r/k_\parallel v_c \simeq 1.2$. At maximum growth the cyclotron

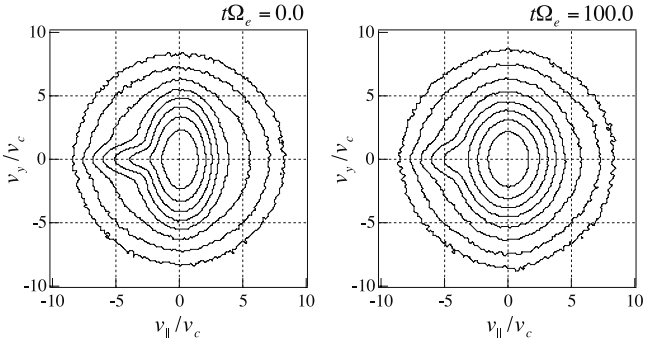

Figure 2. Simulation results for the whistler anisotropy instability run. The electron velocity distribution $\log[f_e(v_\parallel, v_y)/f_e(0, 0)]$ at $t = 0$ and at $|\Omega_e|t = 100$ where $v_\parallel$ and v_y are normalized by v_c, the core thermal speed.

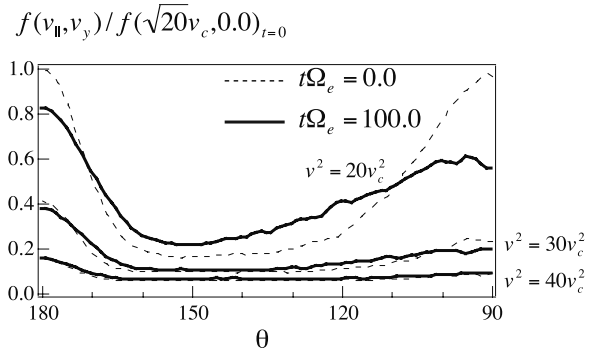

Figure 3. Simulation results for the whistler anisotropy instability run. Electron pitch angle distributions at $t = 0$ (dashed lines) and at $|\Omega_e|t = 100$ (solid lines) for electrons with $v^2 = 20v_c^2$, $30v_c^2$, and $40v_c^2$ as labeled.

resonance factor of the core $\zeta_c^+ = (\omega - k_\parallel v_{oc} + \Omega_e)/\sqrt{2}k_\parallel v_c$ is about 0.9, indicating a strong wave-particle resonance. Thus the whistler anisotropy instability is excited; the fluctuating fields perpendicular to $\mathbf{B}_o$ grow at $\gamma_m/|\Omega_e| \simeq 0.12$ in approximate agreement with linear theory, and reach saturation as illustrated in Figure 1 (top). Figure 1 (bottom) shows the fluctuation spectrum at $|\Omega_e|t = 50$. The enhanced fluctuations lie within $0.5 < kc/\omega_e \lesssim 1.0$, consistent with the predictions of significant wave growth from linear dispersion theory. Spectra at later times, not shown here, show a gradual shift toward smaller wave numbers; e.g., at $|\Omega_e|t = 100$, the enhanced fluctuations lie within $0.4 < kc/\omega_e \lesssim 0.9$.

[12] Figure 2 illustrates the electron velocity distribution at both $t = 0$ and $|\Omega_e|t = 100.0$. The instability is driven by the anisotropic core electrons, and it is those electrons which are most strongly scattered; the sense of the scattering, as is typical for such an incoherent process, is down the gradient of the velocity distribution along a curve of constant energy in the wave frame. The result is to reduce the core anisotropy, as shown in the late-time panel. For the parallel-propagating instability, $\zeta_s^+ \simeq 0.4$, indicating that relatively low-energy strahl electrons are also cyclotron resonant with and scattered by this mode. But the gradient on the strahl velocity distribution points from smaller to larger $v_\perp$ so that, as shown in Figure 2 (right), the low-energy part of this component has a broadened pitch-angle distribution at late times.

[13] This effect is shown more clearly in Figure 3, which illustrates electron pitch-angle distributions for three values of v at initial and late times. The less energetic electrons are more strongly resonant with the relatively short-wavelength enhanced fluctuations and are therefore scattered more strongly; the consequence is to reduce the anisotropies of both the core and the strahl. However, the weakening of the resonance at larger v means that the strahl retains its initial narrow character with increasing electron energy.

3. Simulation: Initial Broadband Fluctuation Spectrum

[14] The simulation described in this section begins with an isotropic core distribution, i.e., $T_{\perp c}/T_{\parallel c} = 1.0$. A broadband spectrum of fluctuations is applied at $t = 0$; the simulation then follows the subsequent temporal evolution of the system. The fluctuating magnetic and electric fields initially imposed upon the system are:

$$\delta\mathbf{B}(x, t = 0) = \sum_{n=1}^{nmax} -\hat{\mathbf{y}}\ \delta B_n \sin(-k_n x + \phi_n) + \hat{\mathbf{z}}\ \delta B_n \cos(-k_n x + \phi_n) \quad (1)$$

$$\delta\mathbf{E}(x, t = 0) = \sum_{n=1}^{nmax} \hat{\mathbf{y}}\ \delta E_n \cos(-k_n x + \phi_n) + \hat{\mathbf{z}}\ \delta E_n \sin(-k_n x + \phi_n) \quad (2)$$

with δB_n as the amplitude of mode n, $\delta E_n = (\omega/kc)\ \delta B_n$, and wave number $k = k_\parallel$ understood. Each mode is a normal mode of the plasma with dispersion properties as given by solutions of the electromagnetic dispersion equation at $\mathbf{k} \times \mathbf{B}_o = 0$ [*Gary*, 1993, chapter 6]. Spatially inhomogeneous velocity perturbations are added to each particle component at $t = 0$ to make the particles more nearly self-consistent with the field fluctuations of equations (1) and (2).

[15] The initial power spectrum is chosen to be

$$\frac{|\delta B(t = 0)|^2}{B_o^2} = S_B \sum_{n=1}^{nmax} (k_n c/\omega_e)^{-\alpha} \quad (3)$$

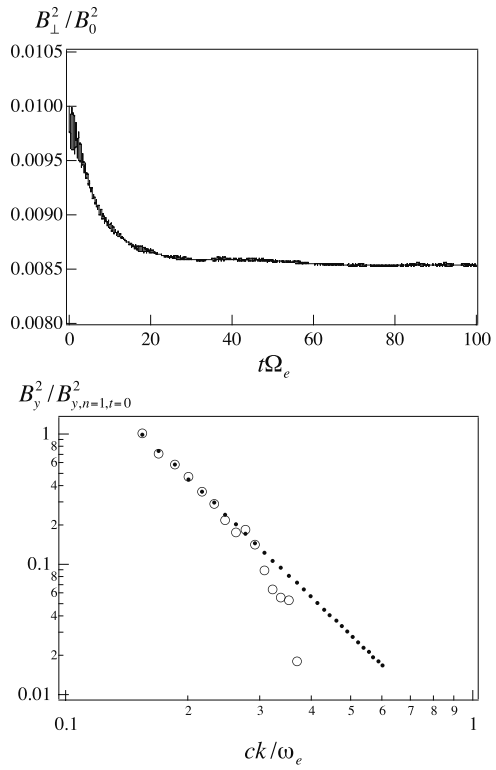

Figure 4. Simulation results for the run with an initially imposed spectrum of broadband fluctuations. (top) The normalized magnetic fluctuation field energy density as a function of time and (bottom) the power spectrum of the y-component of the fluctuating magnetic field at $t = 0$ (solid dots) and at $|\Omega_e|t = 100$ (open circles) as a function of the parallel wave number.

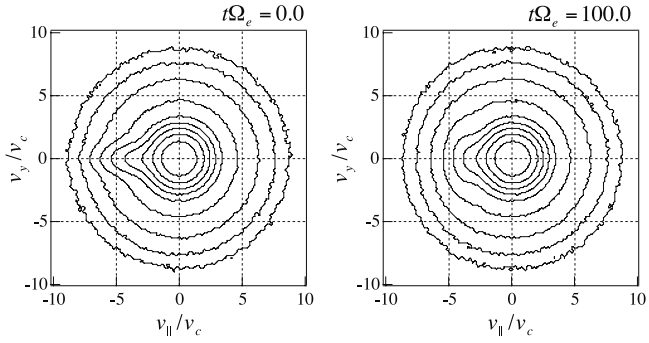

Figure 5. Simulation results for the run with an initially imposed spectrum of broadband fluctuations. The electron velocity distribution $\log[f_e(v_\parallel, v_y)/f_e(0, 0)]$ at $t = 0$ and at $|\Omega_e|t = 100$ where $v_\parallel$ and v_y are normalized by v_c, the core thermal speed.

with $nmax = 30$ whistler modes which are equally spaced in wave number. We further chose $\alpha = 3$ [*Smith et al.*, 2006], $k_1c/\omega_e = 0.153$, $k_{30}c/\omega_e = 0.598$, and $|\delta B(t = 0)|^2/B_o^2 = 0.01$.

[16] Although these modes are discrete, most have a nonzero damping decrement. This means that the resonant velocity factor of each mode $[R_j(v_\parallel) \equiv \Omega_j/(k_\parallel v_\parallel - \omega - \Omega_j)]$ has a finite width in $v_\parallel$ [*Gary and Saito*, 2003]; the velocity overlap of these factors implies that electron scattering by this discrete fluctuation spectrum should emulate the consequences of scattering by the essentially continuous power spectrum of magnetic fluctuations in the solar wind.

[17] Figure 4 (top) shows the temporal evolution of the total fluctuating magnetic field energy for this simulation; there is a modest decrease in $|\delta B|^2/B_o^2$ with time, corresponding to the damping which transfers energy to the electrons, particularly the cyclotron resonant strahl. Figure 4 (bottom) illustrates the initial and final power spectra of the fluctuations; as predicted by linear theory, the short wavelength modes have the strongest damping.

[18] Figure 5 illustrates the electron velocity distribution $f_e(v_\parallel, v_y)$ at $t = 0$ and $|\Omega_e|t = 100$. With our choice of parameters, the initial distribution illustrated in Figure 5 (left) bears a strong resemblance to electron velocity distributions with isotropic halos measured by ACE in the solar wind [*Gosling et al.*, 2001]. A comparison of Figure 5 (left and right) shows evident pitch-angle scattering of the strahl; furthermore, the figure suggests that this scattering is greater at larger electron energies.

[19] This suggestion is borne out by Figure 6 which shows electron pitch-angle distributions from this run at $t = 0$ and at $|\Omega_e|t = 100$ for three different values of v. At the start of the simulation, our choice of a bi-Maxwellian suprathermal velocity distribution corresponds to pitch-angle distributions which become narrower as $|v_\parallel|$ increases. But at late times, the opposite trend is evident; clearly the whistlers have induced a broadening in pitch-angle with increasing electron energy.

[20] Resonant scattering of the suprathermals is sensitive to the choice of initial parameters of the whistler fluctuation spectrum. As suggested by Figure 4 (bottom), the primary dissipation here is due to the relatively short wavelength modes; similar computations not illustrated here which remove short-wavelength modes via the choice of $k_{30}c/\omega_e = 0.25$ yield no discernable decrease in the total fluctuation energy and much less scattering of the strahl.

4. Conclusions and Interpretations

[21] We have used particle-in-cell simulations to compute suprathermal electron responses to electromagnetic fluctuation spectra from two distinct sources: the whistler anisotropy instability driven by $T_\perp/T_\parallel > 1$ on the electron core component, and a broadband power-law spectrum of whistler fluctuations imposed upon the system at $t = 0$. Both simulations show broadening of strahl pitch-angle distributions, providing further evidence that enhanced whistlers are a likely source of scattering for suprathermal electrons in the solar wind. But the two different whistler sources have distinctly different consequences.

[22] The instability-driven fluctuations are enhanced at relatively large wave numbers; such modes mainly scatter the low energy core electrons. Strahl electrons with velocities close to those of the core are also scattered and their pitch-angles are increased, but at higher energies the strahl retains its initial narrow character. Strahl pitch-angle distributions are often observed to become more narrow as electron energy increases (see citations above). Particle-particle collisions become weaker with increasing electron energy, and are a plausible source for this narrowing of the strahl. But *Lemons and Feldman* [1983] have shown that collisions are not always sufficient to describe the observed strahl width, especially at lower energies. Thus, scattering by enhanced fluctuations from the whistler anisotropy instability may also contribute to this characteristic strahl property. Because this instability reduces but does not necessarily eliminate the driving anisotropy, a residual $T_{\perp c}/T_{\parallel c} > 1$ may be an observational indication that this growing mode has contributed to strahl broadening.

[23] The initially-imposed broadband whistlers resonate with and scatter a broader range of strahl; because longer wavelength fluctuations have greater energies, they interact with the faster electrons more strongly, leading to pitch-angle distributions which are broader with increasing electron energy. We assume the breakpoint between the inertial range of solar wind MHD turbulence and the so-called "dissipation" range (or, more accurately, following *Stawicki*

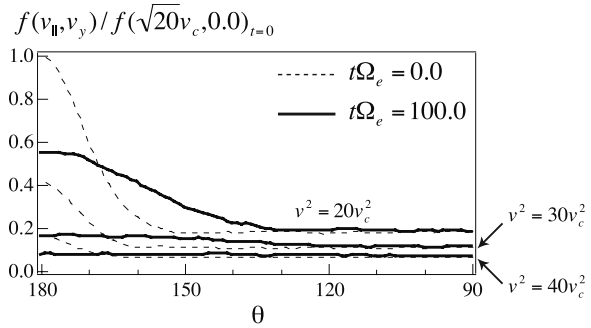

Figure 6. Simulation results for the run with an initially imposed spectrum of broadband fluctuations. Electron pitch angle distributions at $t = 0$ (dashed lines) and at $|\Omega_e|t = 100$ (solid lines) for electrons with $v^2 = 20v_c^2$, $30v_c^2$, and $40v_c^2$ as labeled.

et al. [2001], the "dispersion" range) of whistler turbulence corresponds to $k_{\|c}/\omega_p \simeq 1$. If we further assume that this breakpoint corresponds to the onset of strong scattering to electron isotropy, then the corresponding electron energy at cyclotron resonance is $m_e v_\|^2/2 \simeq (m_p/m_e)^2\ (v_A/c)^2\ (m_e c^2/2)$. For typical solar wind parameters near 1 AU of $B_o = 5$ nT and $n_e = 5$ cm^{-3}, this equation predicts that electrons above about 23 keV should be scattered to isotropy.

[24] **Acknowledgments.** The authors acknowledge useful discussions with Ruth Skoug and John Steinberg. This work was performed under the auspices of the U.S. Department of Energy (DOE) and was supported by the DREAM project of the Laboratory Directed Research and Development Program at Los Alamos, as well as by the Sun-Earth Connection Theory Program and the Solar and Heliospheric Physics SR&T Program of the National Aeronautics and Space Administration.

References

Beinroth, H. J., and F. M. Neubauer (1981), Properties of whistler mode waves between 0.3 and 1.0 AU from Helios observations, *J. Geophys. Res.*, *86*, 7755–7760.

Buneman, O. (1993), Computer space plasma physics, in *Simulation Techniques and Software*, edited by H. Matsumoto and Y. Omura, p. 67, Terra Sci., Tokyo.

Feldman, W. C., J. R. Asbridge, S. J. Bame, M. D. Montgomery, and S. P. Gary (1975), Solar wind electrons, *J. Geophys. Res.*, *80*, 4181–4196.

Feldman, W. C., J. R. Asbridge, S. J. Bame, J. T. Gosling, and D. S. Lemons (1978), Characteristic electron variations across simple high-speed solar wind streams, *J. Geophys. Res.*, *83*, 5285–5295.

Gary, S. P. (1993), *Theory of Space Plasma Microinstabilities*, Cambridge Univ. Press, New York.

Gary, S. P., and S. Saito (2003), Particle-in-cell simulations of Alfvén-cyclotron wave scattering: Proton velocity distributions, *J. Geophys. Res.*, *108*(A5), 1194, doi:10.1029/2002JA009824.

Gary, S. P., and J. Wang (1996), Whistler instability: Electron anisotropy upper bound, *J. Geophys. Res.*, *101*, 10,749–10,754.

Gosling, J. T., R. M. Skoug, and W. C. Feldman (2001), Solar wind electron halo depletions at 90° pitch angle, *Geophys. Res. Lett.*, *28*, 4155–4158.

Hammond, C. M., W. C. Feldman, D. J. McComas, J. L. Phillips, and R. J. Forsyth (1996), Variation of electron-strahl width in the high-speed solar wind: Ulysses observations, *Astron. Astrophys.*, *316*, 350–354.

Lemons, D. S., and W. C. Feldman (1983), Collisional modification to the exospheric theory of solar wind halo electron pitch angle distributions, *J. Geophys. Res.*, *88*, 6881–6887.

Lengyel-Frey, D., R. A. Hess, R. J. MacDowall, R. G. Stone, N. Lin, A. Balogh, and R. Forsyth (1996), Ulysses observations of whistler waves at interplanetary shocks and in the solar wind, *J. Geophys. Res.*, *101*, 27,555–27,564.

Maksimovic, M., et al. (2005), Radial evolution of the electron distribution functions in the fast solar wind between 0.3 and 1.5 AU, *J. Geophys. Res.*, *110*, A09104, doi:10.1029/2005JA011119.

Pagel, C., N. U. Crooker, D. E. Larson, S. W. Kahler, and M. J. Owens (2005), Understanding electron heat flux signatures in the solar wind, *J. Geophys. Res.*, *110*, A01103, doi:10.1029/2004JA010767.

Pagel, C., S. P. Gary, C. A. de Koning, R. M. Skoug, and J. T. Steinberg (2007), Whistler scattering of suprathermal electrons in the solar wind, *J. Geophys. Res.*, doi:10.1029/2006JA011967, in press.

Phillips, J. L., and J. T. Gosling (1990), Radial evolution of solar wind thermal electron distributions due to expansion and collisions, *J. Geophys. Res.*, *95*, 4217–4228.

Phillips, J. L., J. T. Gosling, D. J. McComas, S. J. Bame, and E. J. Smith (1989), ISEE 3 observations of solar wind thermal electrons with $T_\perp > T_\|$, *J. Geophys. Res.*, *94*, 13,377–13,386.

Pierre, F., J. Solomon, N. Cornilleau-Wehrlin, P. Canu, E. E. Scime, J. L. Phillips, A. Balogh, and R. J. Forsyth (1995), Whistler-mode wave generation around interplanetary shocks in and out of the ecliptic plane, *Geophys. Res. Lett.*, *22*, 3425–3428.

Pilipp, W. G., H. Miggenrieder, K.-H. Mühlhäuser, H. Rosenbauer, R. Schwenn, and F. M. Neubauer (1987), Variations of electron distribution functions in the solar wind, *J. Geophys. Res.*, *92*, 1103–1118.

Rosenbauer, H., R. Schwenn, E. Marsch, B. Meyer, H. Miggenrieder, M. D. Montgomery, K. H. Mühlhäuser, W. Pilipp, W. Voges, and S. M. Zink (1977), A survey on initial results of the Helios plasma experiment, *J. Geophys.*, *42*, 561–580.

Smith, C. W., K. Hamilton, B. J. Vasquez, and R. J. Leamon (2006), Dependence of the dissipation range spectrum of interplanetary magnetic fluctuations on the rate of energy cascade, *Astrophys. J.*, *645*, L85–L88.

Stawicki, O., S. P. Gary, and H. Li (2001), Solar wind magnetic fluctuation spectra: Dispersion versus damping, *J. Geophys. Res.*, *106*, 8273–8282.

Vocks, C., and G. Mann (2003), Generation of suprathermal electrons by resonant wave-particle interaction in the solar corona and wind, *Astrophys. J.*, *593*, 1134–1145.

Vocks, C., C. Salem, R. P. Lin, and G. Mann (2005), Electron halo and strahl formation in the solar wind by resonant interaction with whistler waves, *Astrophys. J.*, *627*, 540–549.

S. P. Gary and S. Saito, Space Science and Applications Group, Los Alamos National Laboratory, Mail Stop D466, Los Alamos, NM 87545, USA. (pgary@lanl.gov; ssaito@lanl.gov)